Journal of Orthopaedic Translation 49 (2024) 230–245

Contents lists available at ScienceDirect

Journal of Orthopaedic Translation

journal homepage: www.journals.elsevier.com/journal-of-orthopaedic-translation

Original Article

Engineered melatonin-pretreated plasma exosomes repair traumatic spinal cord injury by regulating miR-138-5p/SOX4 axis mediated microglia polarization

Hao Chen [a,1], Huihui Sun [a,1], Yaqing Yang [b,1], Pingchuan Wang [c], Xizhao Chen [a], Junxiang Yin [a], Aoying Li [a], Liang Zhang [a], Jun Cai [a], Jijun Huang [a], Shengfei Zhang [a], Zhiqiang Zhang [a], Xinmin Feng [a], Jian Yin [d,****], Yongxiang Wang [a,e,f,***], Wu Xiong [g,**], Bowen Wan [a,*]

[a] Department of Orthopedics, Northern Jiangsu People's Hospital Affiliated to Yangzhou University/Clinical Medical College, Yangzhou University, Yangzhou, China
[b] Department of Basic Medical Science, Jiangsu Vocational College of Medicine, Yancheng, China
[c] Department of Orthopedics, Affiliated Hospital of Yangzhou University, Yangzhou, China
[d] Department of Orthopedics, the Affiliated Jiangning Hospital with Nanjing Medical University, Nanjing, China
[e] Department of Orthopedics, the Yangzhou Clinical Medical College of Xuzhou Medical University, Yangzhou, China
[f] Department of Orthopedics, Northern Jiangsu People's Hospital, Affiliated Hospital of Nanjing University Medical School, Yangzhou, China
[g] Department of Orthopedics, The First Affiliated Hospital of Nanjing Medical University, Nanjing, China

ARTICLE INFO

Keywords:
Engineered melatonin-pretreated plasma exosomes
MiR-138-5p/SOX4 axis
Spinal cord injury

ABSTRACT

Background: Neuroinflammation plays a crucial role in the repair of spinal cord injury (SCI), with microglia, pivotal in neuroinflammation, driving either degeneration or recovery in this pathological process. Recently, plasma-derived exosomes (denoted Exos) have presented a high capacity for promoting functional recovery of SCI through the anti-inflammatory effects, and pretreated exosomes are associated with better outcomes. Thus, we aimed to explore whether melatonin-pretreated plasma-derived exosomes (denoted MExo) could exert superior effects on SCI, and attempted to elucidate the potential mechanisms.

Methods: Electron microscopy, nanoparticle tracking analysis, and western blot were applied to delineate the distinctions between Exos and MExos. To assess their therapeutic potentials, we established a contusion SCI rat model, complemented by a battery of in vitro experiments comparing both groups. Subsequently, a miRNA microarray analysis was conducted, followed by a series of rescue experiments to elucidate the specific role of miRNAs in MExos. To further delve into the molecular mechanisms involved, we employed western blot analysis and the luciferase reporter gene assay.

Results: Melatonin promoted the release of exosome from plasma, concurrently amplifying their anti-inflammatory properties. Furthermore, it was discerned that MExos facilitated a transition in microglia polarization from M1 to M2 phenotype, a phenomenon more pronounced than that observed with Exos. In an endeavor to elucidate this variance, we scrutinized miRNAs exhibiting elevated expression levels in MExos, pinpointing miR-138-5p as a pivotal element in this dynamic. Following this, an in-depth investigation into the role of miR-138-5p was undertaken, which uncovered its efficacy in driving phenotypic alterations within microglia. The analysis of downstream genes targeted by miR-138-5p revealed that it exerted a negative regulatory influence on SOX4, which was found to obstruct the generation of M2-type microglia and the secretion of anti-inflammatory cytokines, thereby partially elucidating the mechanism behind miR-138-5p's regulation of microglia polarization.

* Corresponding authors.
** Corresponding author.
*** Corresponding authors. Department of Orthopedics, Northern Jiangsu People's Hospital Affiliated to Yangzhou University/Clinical Medical College, Yangzhou University, Yangzhou, China./ Department of Orthopedics, the Yangzhou Clinical Medical College of Xuzhou Medical University, Yangzhou, China./ Department of Orthopedics, Northern Jiangsu People's Hospital, Affiliated Hospital of Nanjing University Medical School, Yangzhou, China
**** Corresponding author.
E-mail addresses: yinjiandoc@njmu.edu.cn (J. Yin), wyx918spine@163.com (Y. Wang), a1370791271@163.com (W. Xiong), wanbowen@njmu.edu.cn (B. Wan).
[1] These authors contribute equally to this study.

https://doi.org/10.1016/j.jot.2024.09.007
Received 7 March 2024; Received in revised form 8 September 2024; Accepted 25 September 2024

Conclusions: We innovatively observed that melatonin enhanced the anti-inflammatory function of Exos, which further decreased the expression of SOX4 by delivering miR-138-5p. This inhibition promoted the conversion of M1 microglia to M2 microglia, thus offering a viable option for the treatment of SCI.
The translational potential of this article: This study highlights that melatonin enhances the anti-inflammatory function of Exos through delivery of miR-138-5p. Activation of miR-138-5p/SOX4 axis by engineered melatonin-pretreated plasma exosomes may be a potential target for SCI treatment.

1. Introduction

Spinal cord injury (SCI) refers to the spinal cord damage caused by destructive forces. This injury can result in temporary or permanent alterations or loss of spinal cord function [1]. Primary trauma impairs neuroglial cells and neurons, triggering a series of inflammatory cascade reactions over time. Activation of microglia, consequential production of inflammation factors, and infiltration of immune cells are major contributors to secondary injury, leading to the progressive cellular damage and tissue injury [2,3]. The injured site is replaced by cystic cavity and glial scar that hinder neural regeneration, impact motor function, and potentially cause paralysis or death [4]. Therefore, investigation of new therapeutic approaches for SCI is imminent.

Microglia, as key immune constituents of the CNS, orchestrate a series of critical processes that are essential in initiating and moderating the inflammatory response after SCI [5–7]. Their impact on neuroinflammation and neuroregeneration is bimodal and is influenced by their polarization states: either the classically activated M1 or the alternatively activated M2 phenotypes [8,9]. M1 microglia are associated with the release of inflammatory mediators such as TNF-α, IL-1β, and IL-6, which result in inflammatory tissue damage. In contrast, M2 microglia contribute to recovery by producing cytokines and growth factors, namely IL-4, IL-10, and TGF-β, which support the process of neuroregeneration [10,11]. It is therefore imperative that investigative endeavors aim at developing therapeutic approaches that not only promote the shift of microglia polarization from M1 towards M2 but also mitigate the adverse effects of rampant neuroinflammation in the context of SCI treatment [12,13].

Exosomes, ranging in size from 30 to 200 nm, are organelles enclosed by a membrane that can be released by prokaryotic and eukaryotic cells. Exosomes exhibit structural similarities to cells and serve as carriers of a diverse array of molecules such as proteins, lipids, and nucleic acids, playing a pivotal role in influencing the biological activities of their recipient cells [14–17].

Exosomes derived from various sources participate in many diseases including SCI by modulating complex intracellular pathways [18–21]. Literature has also reported that plasma-derived exosomes (Exos) exhibit anti-inflammatory effects and protect the myocardium from ischemia-reperfusion injury [22]. Nevertheless, the low production of the exosomes due to limited cells remains an obstacle for wide use, and the efficacy of exosomes is also to be improved [23]. To overcome this bottleneck, pretreatment methods have been frequently investigated to enhance the functionality and yield of exosomes [24]. Engineered exosomes have gained widespread applications. Atorvastatin-pretreated mesenchymal stem cells (MSCs)-derived exosomes accelerate diabetic wound healing through the AKT/eNOS pathway [25]. Exosomes derived from MSCs preconditioned under hypoxic conditions present enhanced effectiveness in improving functional behavioral recovery compared to normoxic conditions exosomes in post-SCI mice treatments [26]. Previous studies have concluded that pretreatment with melatonin can affect the yield and content of exosomes thereby improving the antioxidant, anti-inflammatory, and anti-apoptotic function [23,27–29]. However, whether plasma-derived exosomes alone or preteatment with melatonin can improve the functional recovery in SCI rats remains unclear.

Given the synergistic anti-inflammatory properties of melatonin and Exos, it was assumed that melatonin-pretreated plasma-derived exosomes (MExos) might regulate neuroinflammation more effectively following SCI. In this study, we observed that melatonin-pretreatment promoted the yield and content of Exos. Through miRNA microarray analysis, miR-138-5p emerged as the most abundant miRNA in MExos, facilitating the shift of microglia polarization from the M1 to M2 phenotype both in vivo and in vitro by suppressing the activity of SOX4. More importantly, engineered MExos that we constructed with excessive miR-138-5p significantly reduced neuroinflammation and improved motor recovery after SCI. This finding demonstrated an underlying mechanism for the application of engineered MExos and presented a potential therapeutic target for SCI (Graphical abstract).

2. Methods

2.1. HAPI and primary microglia culture

Highly aggressively proliferating immortalized (HAPI) rat microglial cells were obtained from American Type Culture Collection (ATCC, USA). Primary microglia (PM) were acquired from 1 to 3 d postnatal Sprague–Dawley (SD) rats as previously reported [30]. Briefly, pups were decapitated, and the entire cortex was carefully dissected from the brain. The blood vessels and meninges were removed completely, and the cortical tissues were sliced into 1 mm × 1 mm fragments, which were then dissociated with 0.25 % trypsin followed by 0.1 % DNase treatment and incubated for 20 min. After digestion, the tissue fragments were centrifuged at 1000 rpm for 5 min. The precipitates were resuspended and cultured in DMEM/F12 in T75 flasks to get primary microglia. Purified microglia were obtained after shaking for 2 h at 120 rpm at 37 °C. The supernatants were collected and placed in poly-L-lysine precoated 6-well plates. The medium was refreshed 4 h for the first time and every 2 d thereafter. The purity of primary microglia is greater than 95 % as determined by immunofluorescence with antibody against Iba1 (Thermo Fisher Scientific).

2.2. Exosome extraction and identification

Melatonin was solubilized in a saline solution (0.9 g/100 mL), supplemented with 5 % dimethyl sulfoxide (DMSO). Subsequently, this solution was administered intraperitoneally at a daily dose of 10 mg/kg for seven consecutive days. Following a seven-day period, plasma samples were collected for analysis. The isolation of extracellular vesicles (EVs), specifically exosomes, was conducted using a comprehensive extracellular vesicle isolation kit. Briefly, after anesthetization, peripheral blood was obtained in tubes with EDTA. The blood samples were centrifuged (1200×*g*, 10 min, 4 °C) immediately to separate the plasma. We carefully transferred the plasma to a new tube. After incubation for 10 min at room temperature, the plasma was centrifuged (3000×*g*, 20 min, 4 °C). Then after another centrifugation step (11000×*g*, 30 min, 4 °C), the supernatant was collected and subsequently transferred to a new tube. The obtained samples were further centrifuged at 18000×*g* for another 30 min at 4 °C. Finally, we collected the supernatant in a new tube and centrifuged it at 100,000×*g* for 2 h at 4 °C to precipitate total EVs in the plasma [31]. Transmission electron microscopy (TEM) was employed to examine the exosomal morphology, whereas the size distribution was detected through nanoparticle-tracking analysis (NTA) [31,32]. Additionally, the protein levels of key extracellular vesicle markers, namely TSG101, CD9, CD63, and CD81, were quantitatively

assessed through western blot (WB) analysis.

2.3. Exosome uptake by microglia

In this study, exosomes were labeled using a 4 mg/mL Dil solution, and subsequently mixed with Phosphate-Buffered Saline (PBS). To remove the excess dye, the exosomes underwent ultracentrifugation at 100,000×*g* for 60 min at temperature under 4 °C. This was followed by three successive PBS washes to purify the Dil-stained extracellular vesicles. Post-labeling, these vesicles were co-cultured with HAPI microglia cells for a period of 24 h. After incubation, microglia were cleansed and fixed in a 4 % paraformaldehyde solution. A confocal laser scanning microscopy was used to examine the absorption of both Dil-labeled Exos and MExos by HAPI microglia, and the fluorescence intensity of Dil was measured with ZEN lite software [26].

Additionally, for flow cytometric analysis, microglia cells were seeded at a density of 15000 cells/well in 24-well plates. After 24 h, cells were incubated with PKH67-labeled Exos and MExos for 8 h and 24 h. Subsequently, cells were washed with PBS, washed with acid wash buffer (0.5 M NaCl, 0.2 M acetic acid) to remove membrane-bound exosomes and once more with PBS. Cells were trypsinized, fixated in 0.2 % paraformaldehyde in PBS and subjected to flow cytometric analysis on a FACSCanto (BD Biosciences).

2.4. Loading miR-138-5p mimics/inhibitors into MExos through electroporation

In the experimental procedure, the mimics and inhibitors of miR-138-5p were incorporated into MExos through electroporation, utilizing the CUY21EDIT II system (BEX, Japan). MiR-138-5p mimics/inhibitors was mixed with MExos on PBS at a ratio of 1:1 (w/w), ensuring the final concentration of MExos in the solution was 0.1 mg/mL. This electroporation mixture was then poured into a cold electroporation cuvette. The parameters were set as follows: 10 cycles of perforation at 110 V, a pulse duration of 6 ms, an interval between pulses of 10 ms, a maintenance voltage of 25 V, and a capacitance of 940 μF. Following electroporation, the mixture was immediately transferred to a fresh tube and incubated for 30 min. To eliminate any unbound mimics or inhibitors, the mixture was subsequently ultracentrifuged at 140,000 g for 70 min and the precipitates were resuspended in PBS.

2.5. Quantitative real-time polymerase chain reaction (qRT-PCR)

TRIzol® method (Invitrogen, USA) was applied to extract total RNA from both cellular and tissue samples. A reverse transcription system (Toyobo, Japan) was used to synthesize cDNA. The Applied Biosystems' SYBR Green PCR Master Mix (Foster City, CA) facilitated the qRT-PCR analyses on an ABI 7900 Fast Real-Time PCR System (Applied Biosystems, Carlsbad, USA). The $2^{-\Delta\Delta CT}$ method was utilized to quantify the relative gene expression levels. β-actin or U6 was selected as internal control genes. Details of the primer sequences are presented in Additional file 1: Table S1.

2.6. Western blot (WB)

RIPA lysis buffer with a protease inhibitor was utilized to extract proteins from spinal cord tissues and/or cultured cells [31]. BCA assay was utilized to detect the concentration of the proteins. Equal amounts of proteins were resolved on SDS-PAGE gels, and PVDF membranes were used for transfer. The membranes were blocked with 5 % BSA to prevent non-specific binding and then incubated with primary antibodies overnight at 4 °C. Next day, the membranes were incubated with secondary antibodies at room temperature for 2 h. ECL reagent (Thermo Fisher Scientific) was applied for protein visualization, and ImageJ software (National Institutes of Health, USA) were applied for protein quantification.

2.7. Luciferase reporter gene assay

GeneScript (Nanjing, China) synthesized the 3′-UTR sequences of SOX4 mRNA, encompassing both wild-type (WT) and mutant (MUT) binding sites. These sequences were integrated into pGL3 luciferase reporter vectors (Promega, USA) using FseI and XbaI sites, resulting in the creation of 3′-UTR reporter constructs for SOX4 (pGL3-WT-SOX4 and pGL3-MUT-SOX4). Either miR^{OE} or a negative control was transfected into HAPI and primary microglia, which were then placed in 96-well plates. Subsequently, 100 ng of either the pGL3-WT-SOX4 or pGL3-MUT-SOX4 3′-UTR were co-transfected into the cells. The Dual-Luciferase® Reporter Assay System (Promega, USA) was applied to measure the dual-luciferase signals.

2.8. Enzyme linked immunosorbent assay (ELISA)

Briefly, the spinal cord tissues were homogenized and lysed, and then centrifugation at 3000 rpm for 30 min was conducted to collect the supernatants. ELISA kits were utilized to detect the concentrations of inflammatory cytokines in the culture supernatants of HAPI microglia and PM, as well as in the aforementioned tissue homogenates, following manufacturer guidelines. A microplate reader was utilized to measure the measurement of optical density or fluorescence.

2.9. Fabrication of rat model of contusion SCI

Animal experiments were granted by the Animal Care and Use Committee of Northern Jiangsu People's Hospital. SD rats were purchased from the Animal Experimental Center of Yangzhou University. In line with prior research [33], rats (220–240 g) were anesthetized with 1 % pentobarbital sodium (50 mg/kg) via intraperitoneal injection, and their intact dorsal cord surfaces were exposed by laminectomy at T10 (the tenth thoracic vertebra). Subsequently, a weight-drop impact (RWD, CA, USA, 68097) was performed using a 10 g rod (2.5 mm in diameter) dropped from a height of 12.5 mm. Signs of successful model establishment included hind limb extension and tail-flick reflex. Postoperative care included twice-daily manual bladder evacuation until spontaneous urination was restored.

2.10. Functional locomotor score

The Basso, Beattie, and Bresnahan (BBB) assessment evaluates limb movements in an open field, encompassing joint mobility, weight-bearing ability, plantar walking, coordination, forelimb positioning, trunk stability, and tail control. The test scores range from 0 to 21, with 0 indicating complete hind limb paralysis and 21 representing normal movement. The objective of the BBB test is to evaluate general fundamental motor skills. Each rat was placed in a spacious area, where two researchers, who were unaware of the experimental group, observed the rat for over 3 min. Before modeling, every rat underwent an evaluation to confirm the absence of any initial abnormalities, and the scores from each session were combined to calculate the final score.

2.11. Footprint analysis

The front and back legs of the rat were individually submerged in blue and red dyes separately. Measurements and analysis of their stride length and width were conducted only when the rats were running at a consistent pace. Two assessors, who were unaware of the experimental protocol, independently evaluated each rat.

2.12. Swimming score

Rats were arranged to undergo swimming tests following SCI. Then, the rats were positioned in a tank filled with water, motivated to move across the entire length, and their swimming positions were

documented. To evaluate the restoration of motor function in rats, the Louisville Swimming Scale (LSS) was employed.

2.13. Electrophysiology

Electromyography (EMG) was employed to measure the motor-evoked potentials (MEPs) in rats 28 d after SCI. For this procedure, the spinal cord was exposed, and the stimulation electrodes were positioned on its outer surface, with recording electrodes connected to the biceps femoris flexor muscle. The distal tendon of the hindlimb muscle was connected to the reference electrode and the ground electrode was inserted subcutaneously. Nerve conduction efficacy in the rats' hindlimbs was assessed by measuring the peak-to-peak amplitude following a singular square wave stimulus.

2.14. Magnetic resonance imaging (MRI)

For MRI examinations, three rats from each group were randomly selected. A mixture of isoflurane (3–4% for induction and 1.5–2% for maintenance), oxygen (0.4 L/min) and nitrogen (0.6 L/min) was used for anesthesia. The models were fixed on a stabilizing apparatus in prone position and scanned using a compact animal MRI system (Bruker BioSpec 7 T/20 USR, Germany). ParaVision 6.0.1 software (Bruker BioSpec, Germany) facilitated the acquisition of T2-weighted images. T2 is one of the two principal relaxation times in MRI. FireVoxel (CAI2R, NY) was used to evaluate and compare the progression of hyperintense signals and lesion volume, which was achieved by summing the areas of individual slices and then multiplying by the combined thickness of a 1.0 mm slice and the intervening gap. The quantitative assessment involved calculating the intensity ratio, contrasting the signal from the lesion region with that of unaffected cord tissue distant from the injury site.

2.15. Immunofluorescence (IF) staining

At the scheduled time points, spinal cord tissues and/or isolated cells were fixed using 4 % PFA, and blocked in 10 % BSA for 1 h. Then, the tissues and/or cells were incubated overnight at 4 °C with primary antibodies: Iba1 (1:1000, mouse lgG; Thermo Fisher Scientific), iNOS (1:250, rabbit IgG; Thermo Fisher Scientific), Arg1 (1:250, rabbit IgG; Cell Signal Technology), MBP (1:1000, mouse lgG; Abcam), and NF200 (1:50, rabbit lgG; Abcam). Immunolabeled tissues and/or cells were incubated with FITC- or Cy3-conjugated secondary antibody (1:200, Jackson ImmunoResearch, USA) for 1 h under darkness. Then, DAPI was utilized to counter stain the nuclei and the fluorescent images were taken.

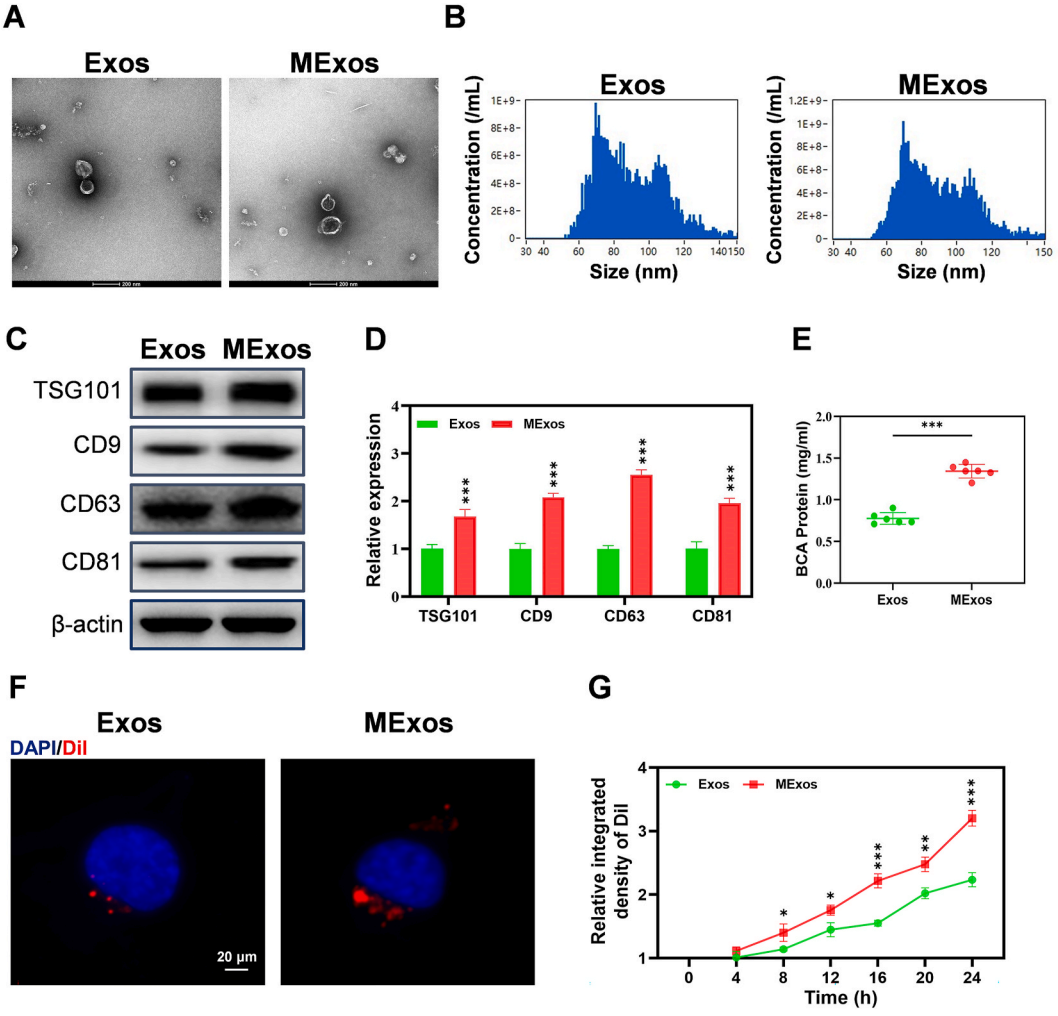

Fig 1. Identification and comparison of Exos and MExos. **A** Morphological observation of Exos and MExos using TEM. **B** Diameter distribution of Exos and MExos identified by NTA. **C** Surface marker detection of Exos and MExos using WB. **D** Relative expression of the proteins as measured by WB. **E** Protein concentration detection of Exos and MExos using BCA assay. **F** Phagocytosis of Exos and MExos by HAPI microglia cells. **G** Comparisons on fluorescence intensity between Exos and MExos groups at indicated time point. *p < 0.05, **p < 0.01, ***p < 0.001.

2.16. Statistical analysis

All experiments were conducted with a minimum of three independent biological replicates. Data was presented as mean ± standard deviation (SD). Statistical analyses were conducted using GraphPad software version 8.0, employing Student's t-test for two-group comparisons and one-way or two-way ANOVA for multi-group comparisons, followed by p-value calculations. A p-value less than 0.05 was considered statistically significant.

3. Results

3.1. Identification and comparison of Exos and MExos

We injected melatonin into rats and isolated exosomes from autologous plasma for identification. TEM showed no apparent morphological differences between Exos and MExos (Fig. 1A). NTA revealed similar diameter distributions for the two groups of exosomes (Fig. 1B). Notably, upon conducting WB analysis to confirm the surface markers of exosomes, we observed a notable rise in the protein composition of MExos (Fig. 1C and D, $p < 0.001$). Furthermore, MExos exhibited a considerably elevated protein concentration compared to the untreated group, suggesting that the administration of melatonin boosted the secretion of exosomes from the plasma (Fig. 1E, $p < 0.001$). Additionally, exosomes labeled with Dil were incubated together with HAPI microglia for a duration of 24 h. Through laser confocal microscopy, we observed the presence of these exosomes within the microglia cytoplasm. Our data from immunofluorescence revealed a time-dependent variation in the phagocytic activity of HAPI microglia towards both Exos and MExos, with a marked increase in MExos ingestion after 8 h (Fig. 1F and G, $p < 0.05$). This result was also confirmed using flow cytometry (Additional file 2: Figs. S1A and B).

3.2. MExos promote the functional behavior recovery after SCI

Melatonin and Exos both exhibit anti-inflammatory effects. Therefore, we hypothesize that MExos can alleviate neuroinflammation and promote the recovery of functional behavior after SCI. To validate this hypothesis, the functional behavior experiments were carried out at scheduled time points after SCI (Fig. 2A). BBB scores and footprint analyses demonstrated improved motor function with Exos and MExos treatments. Notably, the recovery of BBB scores (Fig. 2B, $p < 0.05$ at day 7, $p < 0.01$ at day 14&21, $p < 0.001$ at day 28) and coordination of both forelimbs and hindlimbs (Fig. 2C and D, $p < 0.001$) were more pronounced in the MExos group. MRI examination of the lesion site showed that the area of contusion edema region and the calculated lesion volume (Fig. 2E and F, $p < 0.05$) were the smallest in the MExos group. Moreover, MEP amplitude measurements during electrophysiological assessments of SCI rats showed a significant increase in the Exos and MExos groups, with the latter exhibiting a more pronounced improvement (Fig. 2G and H, $p < 0.001$). The LSS further underscored this trend, demonstrating superior outcomes in the MExos group, thereby affirming more effective motor function recovery post-SCI (Fig. 2I and J, $p < 0.01$). Furthermore, to examine the levels of demyelination in residual or regenerated axons, we performed a dual staining using the 200 kDa neurofilament subunit (NF200) and myelin basic protein (MBP). We observed a marked reduction in the intensity of NF200 and MBP near the injury site compared to regions farther away from the trauma in the Saline-treated group. Notably, the Exos and MExos groups showed a significant decline in this reduced intensity, particularly in the MExos group, as illustrated in Fig. 2K and L ($p < 0.001$). Collectively, these findings underscore the enhanced efficacy of MExos over Exos in promoting functional behavior recovery following SCI.

3.3. MExos reprogram microglia polarization from M1 to M2 phenotype in vivo

ELISA analysis was conducted to measure proinflammatory and anti-inflammatory mediators in the spinal cord three days after SCI. Both Exos and MExos therapies reduced proinflammatory cytokines levels and increased anti-inflammatory cytokines expressions, with MExos showing a more noticeable effect (Fig. 3A, $p < 0.01$). WB and qRT-PCR analyses revealed a notable decrease in M1 phenotype markers ($p < 0.05$) and a corresponding increase in M2 markers ($p < 0.01$) in the Exos and MExos groups in comparison with the Saline group. This effect was particularly pronounced in the MExos group, as depicted in Fig. 3B–D. Meanwhile, in the study illustrated by Fig. 3E and F, the count of Iba1-positive microglia remained consistent across all three examined groups ($p > 0.05$). Yet, there was a discernible decrease in the population of iNOS-positive microglia ($p < 0.001$) and a concurrent increase in Arg1-positive microglia ($p < 0.001$) in proximity to the injury site at day 3 post-SCI in both the Exos and MExos groups, in contrast to the Saline group. Notably, the MExos group demonstrated a trend towards a lower count of iNOS-positive microglia ($p < 0.001$) and a higher count of Arg1-positive microglia ($p < 0.001$), when compared to the Exos group. Taken together, these findings suggest that MExos treatment significantly alters the balance between anti-inflammatory and proinflammatory microglia following SCI, potentially reprogramming microglia polarization from M1 to M2 phenotype in vivo.

3.4. MExos reprogram microglia polarization from M1 to M2 phenotype in HAPI microglia and primary microglia

In vitro experiments were performed to validate the effects of MExos on microglia polarization. After inducing an inflammatory environment using LPS, PBS, Exos, or MExos were added to the culture systems. ELISA results showed a reduction in proinflammatory cytokines and an increase in anti-inflammatory cytokines in both Exos and MExos treated groups, with a stronger effect observed in MExos (Fig. 4A and C, $p<0.05$). Furthermore, Exos and MExos reduced the expression of M1 markers (iNOS, TNF-α, IL-1β) and increased M2 markers (Arg1, CD206, YM1/2), with MExos showing more efficacy (Fig. 4B and D, $p < 0.01$). WB and immunofluorescence analyses corroborated these findings (Fig. 4E–H, $p < 0.01$), confirming the role of MExos in promoting M2 polarization in vitro.

3.5. MiR-138-5p is upregulated in MExos

The in vivo and in vitro analysis revealed that MExos promoted functional recovery and shifted the microglia from M1 to M2 phenotype. Acknowledging the critical role of miRNAs in exosomal functionality, we acquired miRNA profiles from both Exos and MExos. These profiles were obtained from the Gene expression omnibus (GEO) database (GSE147578). As depicted in Fig. 5A, we concentrated on miR-138-5p, which displayed the most significantly upregulated in MExos. The expression of miR-138-5p was achieved through qRT-PCR analysis (Fig. 5B, $p < 0.001$). To explore deeper into the possibility of MExos influencing microglia polarization via miR-138-5p, we constructed both a miR-138-5p mimic and inhibitor, along with respective negative controls. Subsequently, these were integrated into MExos through electroporation, resulting in four distinct variants: miR^{OE}-MExos, $miR\text{-}NC^{OE}$-MExos, miR^{KD}-MExos, and $miR\text{-}NC^{KD}$-MExos, to further assess their regulatory impacts. The loading efficiency was confirmed using qRT-PCR analysis (Additional file 3: Fig. S2).

3.6. MExos reprogram microglia polarization from M1 to M2 phenotype through delivering miR-138-5p in vivo

In vivo, a series of experimental protocols were deployed to elucidate the impact of miR-138-5p on the functional behavior recovery and

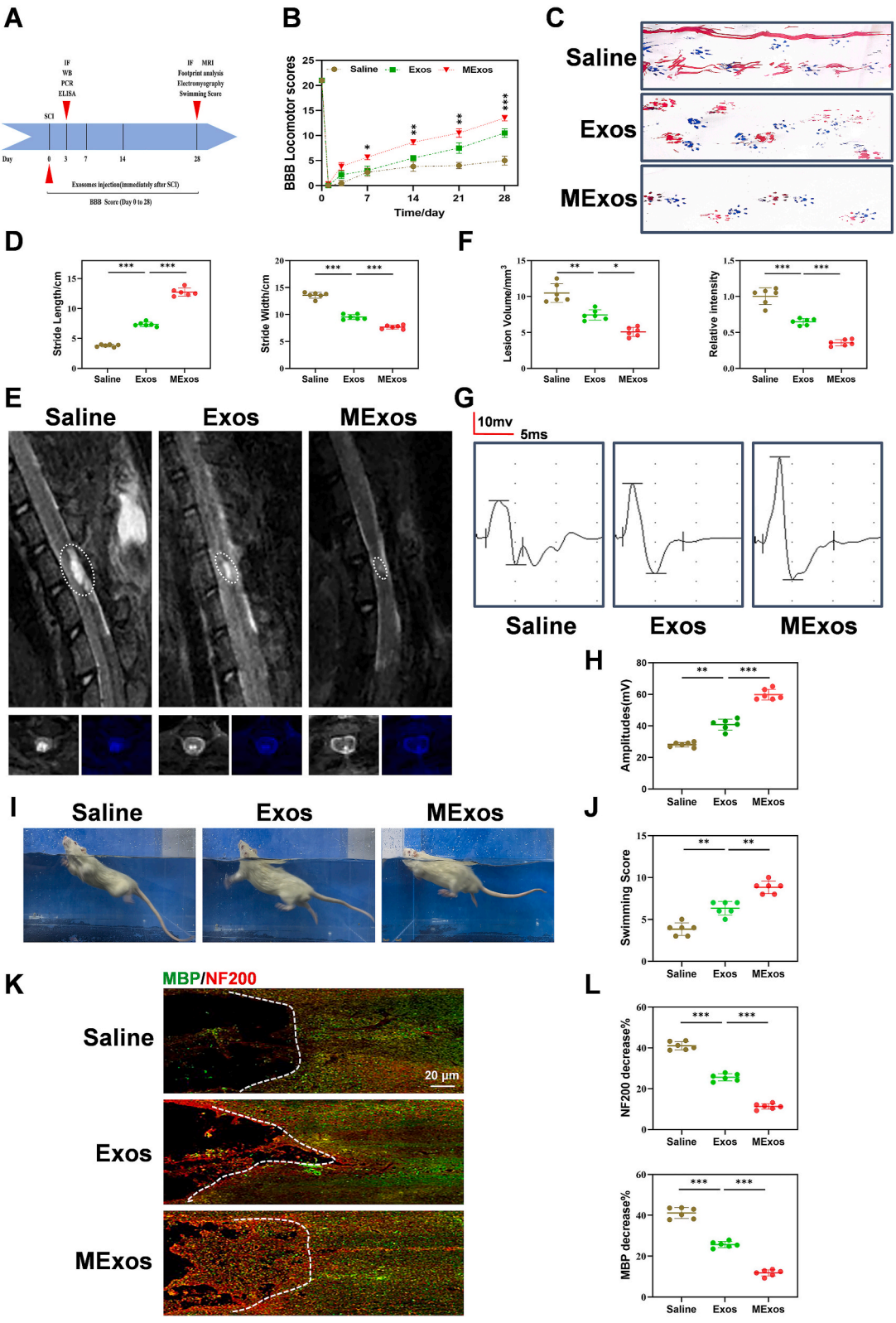

Fig 2. MExos improve the motor function recovery of SCI rats. **A** The functional behavior experiments were carried out at scheduled time points after SCI. **B** Observation of motor function recovery in rats using the BBB score. **C, D** Footprint analysis to assess coordination and motor function in rats, and stride length and width were compared. Forepaw prints were shown in blue and hindpaw prints in red. **E** Representative MRI images of sagittal and axial sections of the injury sites. **F** Relative signal intensity of injured lesion to distant normal tissue and lesion volume calculated by consecutive slices at 28 d post-injury. **G** Analysis of MEP to assess motor recovery in rats. **H** Amplitudes of the rats in each group. **I** Evaluation of motor function recovery in rats through swimming scores. **J** Swimming score of the rats in each group. **K** Immunofluorescence staining for MBP (green) and NF200 (red) to evaluate the extent of demyelination in each group. The white dotted line indicates the borderline of the lesion area. **L** Comparisons on the declining levels of NF200 and MBP among saline, Exos, and MExos groups. The data are plotted as the relative ratio of the immunoreactivity near the injury site compared with that in distant area. *p < 0.05, **p < 0.01, ***p < 0.001.

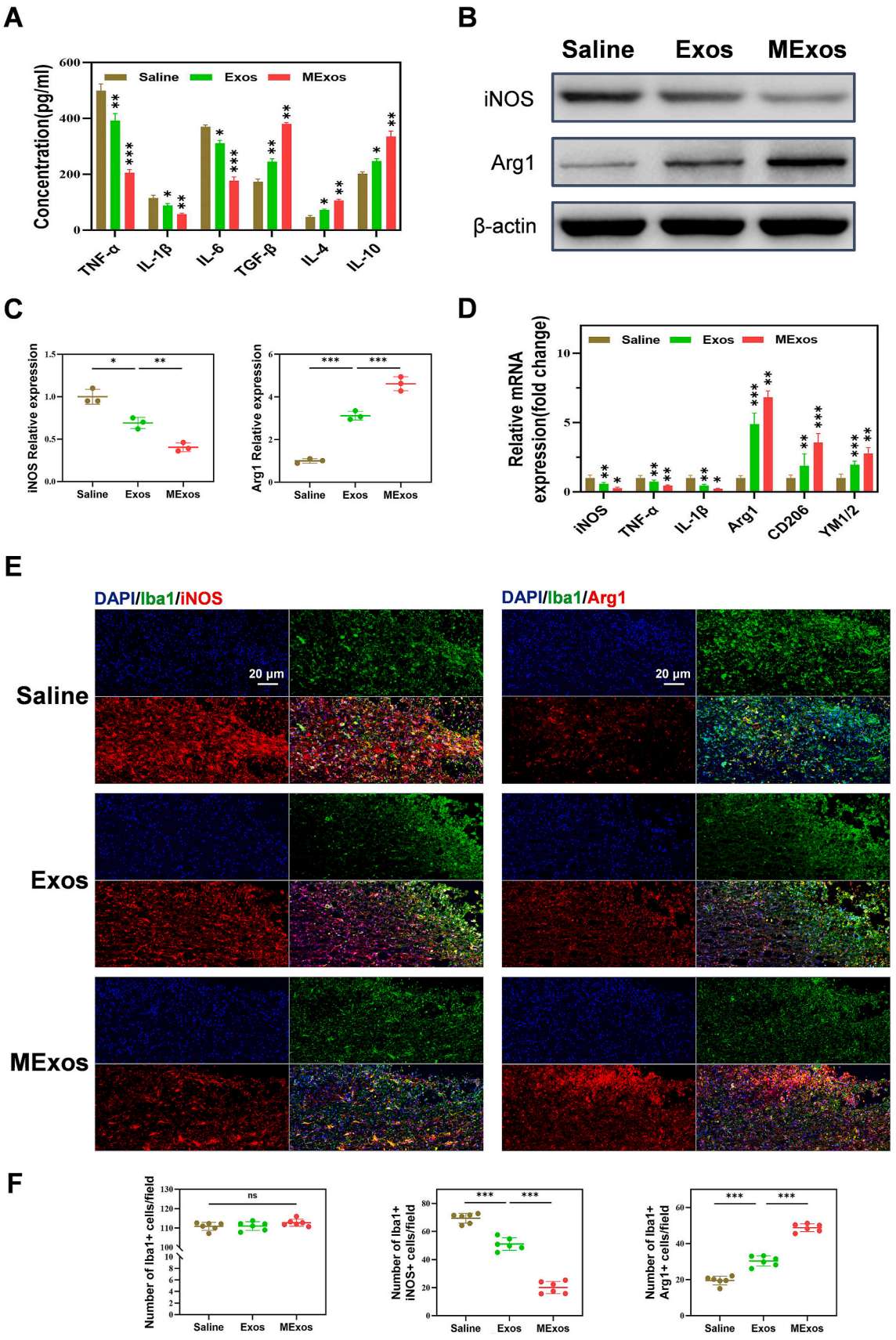

Fig 3. MExos reprogram microglia polarization from M1 to M2 phenotype in rat models. **A** Assessment of inflammatory cytokines after treatment with three different approaches by ELISA. **B, C** Assessment of the expression levels of M1/M2 specific biomarkers in microglia by WB. **D** qRT-PCR analysis of mRNA levels of M1/M2 related markers in microglia. **E, F** Immunofluorescence staining and quantification of M1 (iNOS+/Iba1+) and M2 (Arg1+/Iba1+) microglia in the lesion area. *p < 0.05, **p < 0.01, ***p < 0.001, ns = no significance.

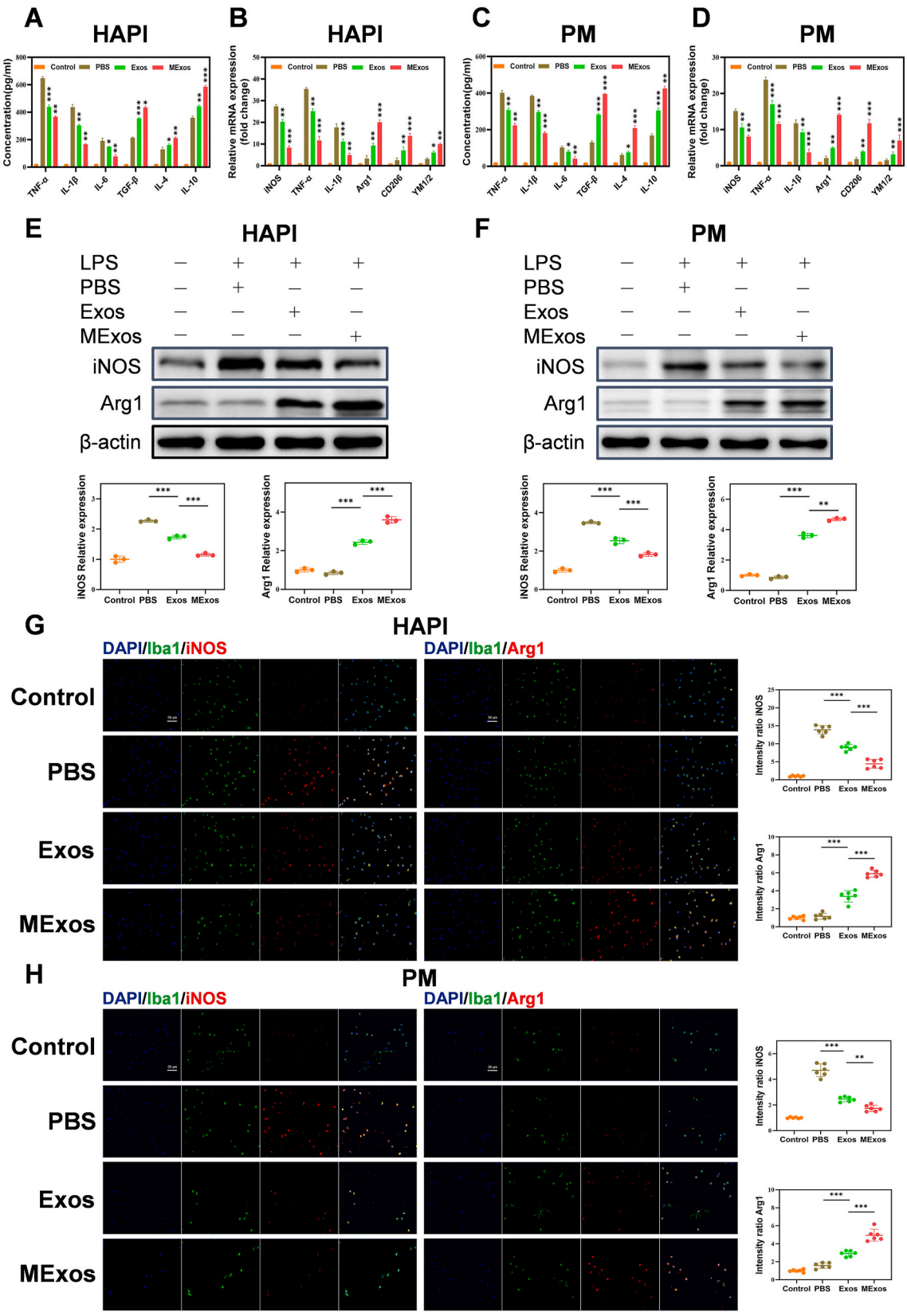

Fig 4. MExos reprogram microglia polarization from M1 to M2 phenotype in HAPI microglia and primary microglia. **A** ELISA was performed to examine the concentrations of inflammatory cytokines in HAPI microglia across four distinct groups. **B** The expression of genes associated with M1 and M2 phenotypes in HAPI microglia of each group were quantified through qRT-PCR. **C** ELISA was employed to examine the levels of inflammatory cytokines in PM from the four experimental groups. **D** qRT-PCR was utilized to detect the mRNA expression of M1/M2 markers in PM across the four groups. **E, F** WB analysis was conducted to assess the protein levels of Arg1 and iNOS in both HAPI and PM. **G, H** The immunofluorescence intensity of iNOS and Arg1 in HAPI and PM for each group was quantified and analyzed. *p < 0.05, **p < 0.01, ***p < 0.001.

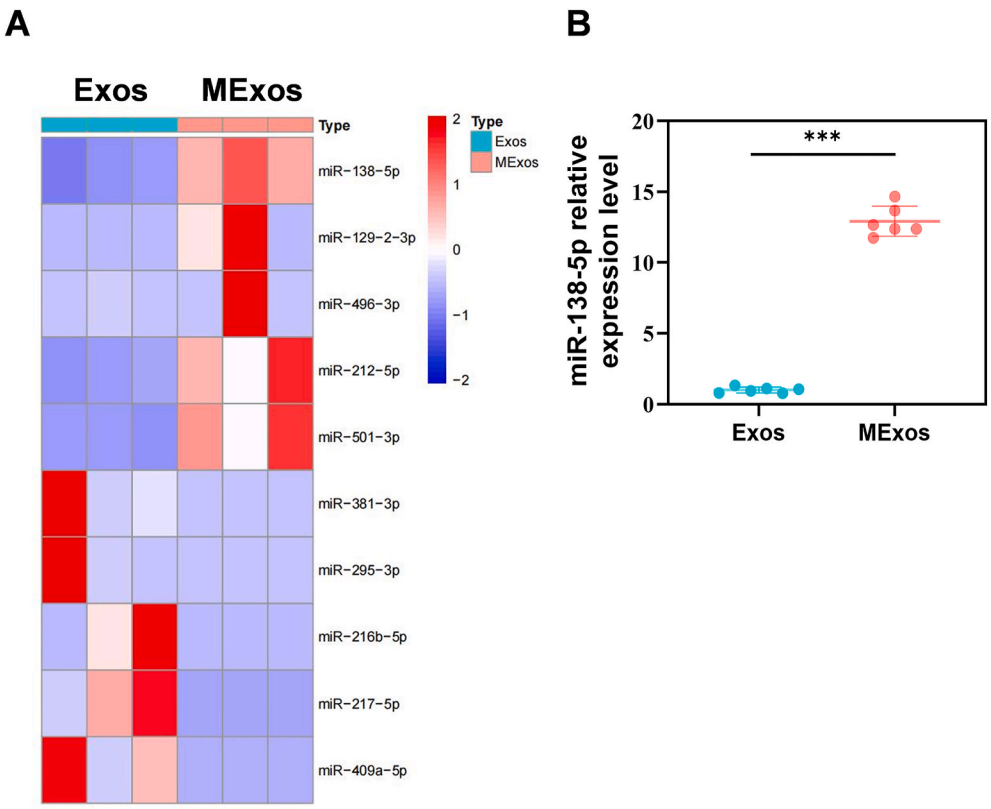

Fig 5. MiR-138-5p is upregulated in MExos. **A** GEO database (GSE147578) identified miR-138-5p as the most enriched miRNA in MExos. **B** The relative expression levels of miR-138-5p in Exos group and MExos group.

microglia polarization mediated by MExos. Preliminary studies, including a range of functional behavioral assessments such as BBB scores, MEP tests, and LSS evaluations, indicated a marked improvement in functional behavior recovery post-administration of miR-138-5p mimic MExos (miR^{OE}-MExos). In contrast, the use of miR-138-5p inhibitor MExos (miR^{KD}-MExos) appeared to reverse the beneficial functional effects typically observed with the MExos group (Additional file 4: Fig. S3). These findings collectively suggest that the facilitation of functional behavior recovery by MExos is largely attributable to the delivery of miR-138-5p.

Subsequently, the research concentrated on unraveling the functional significance of miR-138-5p in regulating microglia polarization, providing further insights into the underlying mechanisms of action. ELISA findings indicated that miR^{OE}-MExos treatment resulted in a notable decrease in the expression of TNF-α ($p < 0.01$), IL-1β ($p < 0.01$), and IL-6 ($p < 0.001$) while showing a considerable increase in the expression of TGF-β ($p < 0.001$), IL-4 ($p < 0.01$), and IL-10 ($p < 0.01$) when compared to the control group (Fig. 6A). Conversely, treatment with miR^{KD}-MExos yielded opposite results (Fig. 6C, $p < 0.01$). The results of qRT-PCR (Fig. 6B) and WB (Fig. 6E) showed that the expressions of M1 phenotype markers were reduced ($p < 0.05$) and M2 phenotype markers were upregulated ($p < 0.01$) in spinal cord tissue of the miR^{OE}-MExos groups compared with that in the miR-NC^{OE}-MExos groups. Conversely, miR^{KD}-MExos produced the opposite effects (Fig. 6D and F). Similar patterns were confirmed through subsequent immunofluorescence staining (Fig. 6G and H, $p < 0.001$). These findings collectively indicate that MExos effectively promoted the transition of microglia from M1 to M2 phenotype following SCI through the transport of miR-138-5p.

3.7. MExos drive microglia reprogramming from M1 to M2 type in both HAPI and primary microglia through miR-138-5p

In order to decipher the mechanism by which MExos facilitate miR-138-5p transfer to modulate microglia polarization, a comprehensive suite of in vitro investigations was conducted on HAPI microglia and PM cultures. Employing ELISA, we observed a notable reduction in proinflammatory cytokines and an upregulation of anti-inflammatory cytokines in the miR^{OE}-MExos treated group (Fig. 7A, $p < 0.01$; Fig. S4C, $p < 0.05$). Contrastingly, the administration of miR^{KD}-MExos yielded inverse results (Fig. 7C, $p < 0.05$; Fig. S4A, $p < 0.05$). Complementary findings from qRT-PCR, WB analyses, and immunofluorescence studies further corroborated that miR^{OE}-MExos treatment induced a shift from the M1 to M2 phenotype in HAPI microglia (Fig. 7B, $p < 0.05$; Fig. 7E, $p < 0.05$; Fig. 7G, $p < 0.001$) and PM (Fig. S4D, $p < 0.01$; Fig. S4F, $p < 0.01$; Fig. S4H, $p < 0.01$) cultures. Conversely, miR^{KD}-MExos treatment exhibited an antagonistic effect in PM (Fig. 7D, $p < 0.01$; Fig. 7F, $p < 0.05$; Fig. 7H, $p < 0.001$) and HAPI microglia (Fig. S4B, $p < 0.01$; Fig. S4E, $p < 0.05$; Fig. S4G, $p < 0.05$) cultures. Collectively, these findings substantiate the role of MExos in steering the polarization shift from M1 to M2 phenotype in both HAPI and primary microglia, mediated via miR-138-5p in vitro.

3.8. MiR-138-5p negatively regulates SOX4 expression in MExos

MiRNAs can exert their functions by inhibiting downstream target genes. In order to delve deeper into the precise mechanism by which miR-138-5p regulates microglia polarization, we conducted a study on the possible target genes that miR-138-5p affects. According to the online database of miRNA targets, it was found that miR-138-5p could potentially target the gene SOX4 (Additional file 6: Fig. S5). In order to confirm whether miR-138-5p can selectively attach to the non-coding area of SOX4, we created wild-type (WT) and mutated (MUT)-3′UTR

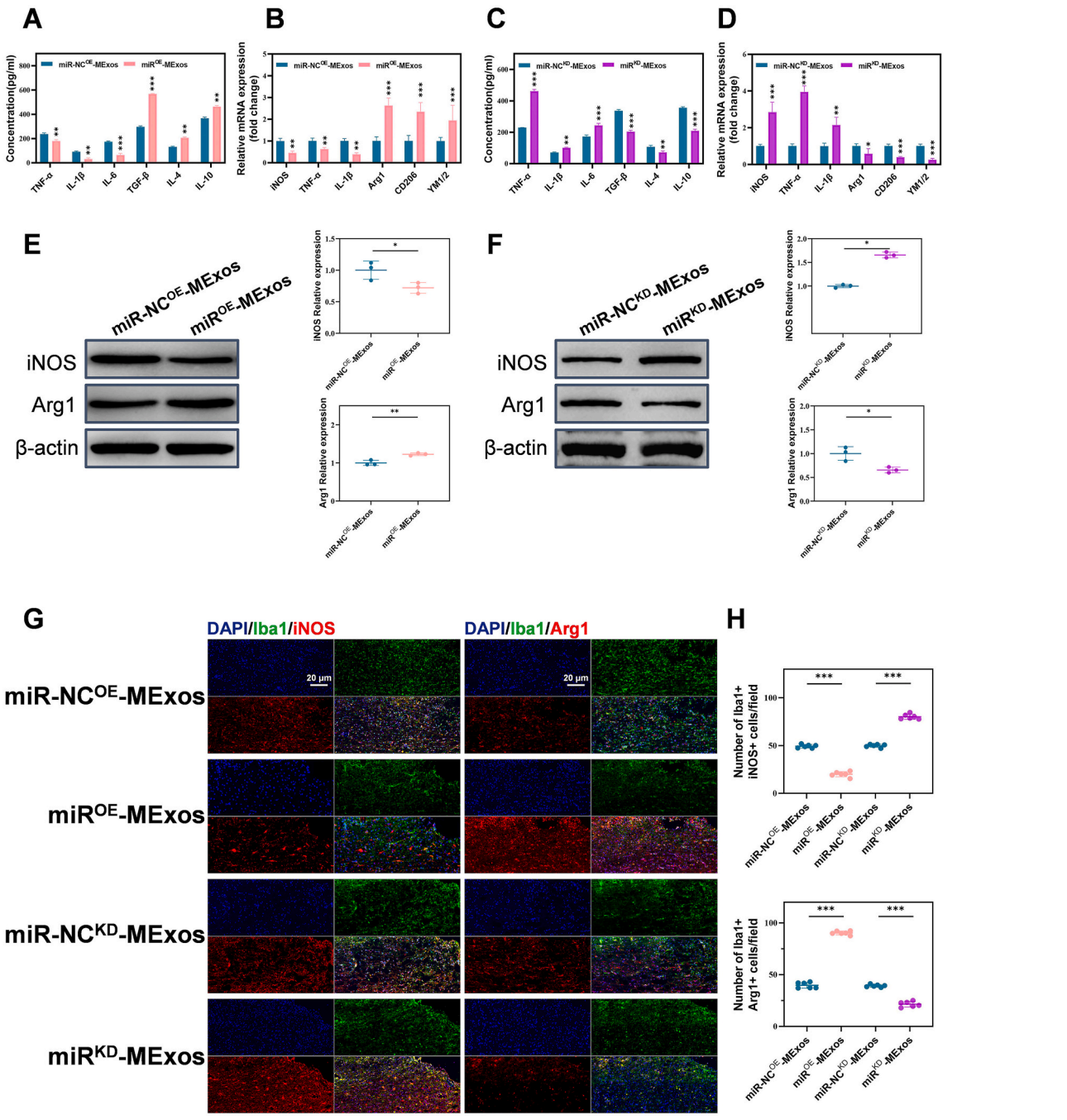

Fig 6. MExos reprogram microglia polarization from M1 to M2 phenotype through transporting miR-138-5p in vivo. **A, C** ELISA was applied to assess the concentrations of inflammatory cytokines in the injured spinal cord of rat models in the four groups. **B, D** The representative gene levels of M1/M2 microglia were evaluated through qRT-PCR in the four groups. **E, F** WB was carried out to assess the levels of M1/M2 specific proteins in the four groups. **G, H** Representative immunofluorescence images and quantitative analysis of M1/M2 specific markers near the lesion sites three days after SCI. *p < 0.05, **p < 0.01, ***p < 0.001.

sequences of SOX4 (Fig. 8A) and examined them using a dual-luciferase reporter test. Overexpression of miR-138-5p was found to significantly attenuate luciferase activity when co-transfected with the SOX4 WT-3′UTR into HAPI microglia and PM, in stark contrast to the observations in the control cohort (Fig. 8B, $p < 0.001$). Interestingly, the suppressive impact of miR-138-5p on luciferase activity was not evident in the context of co-transfection with the SOX4 MUT-3′UTR (Fig. 8B, $p > 0.05$). Then, the results of WB showed that miR-138-5p overexpression decreased SOX4 protein levels and that inhibition of miR-138-5p increased SOX4 protein expressions (Fig. 8C and D, $p < 0.01$) in both HAPI microglia and PM, which further confirmed that SOX4 was the downstream target gene of miR-138-5p.

3.9. MiR-138-5p in MExos regulates M1/M2 polarization of microglia in vitro by targeting SOX4

In this study, the specific interaction between miR-138-5p and SOX4 was confirmed, and we further investigated the impact of SOX4 on microglial polarization through a series of in vitro experiments. By employing lentiviral-mediated SOX4 overexpression and shRNA-

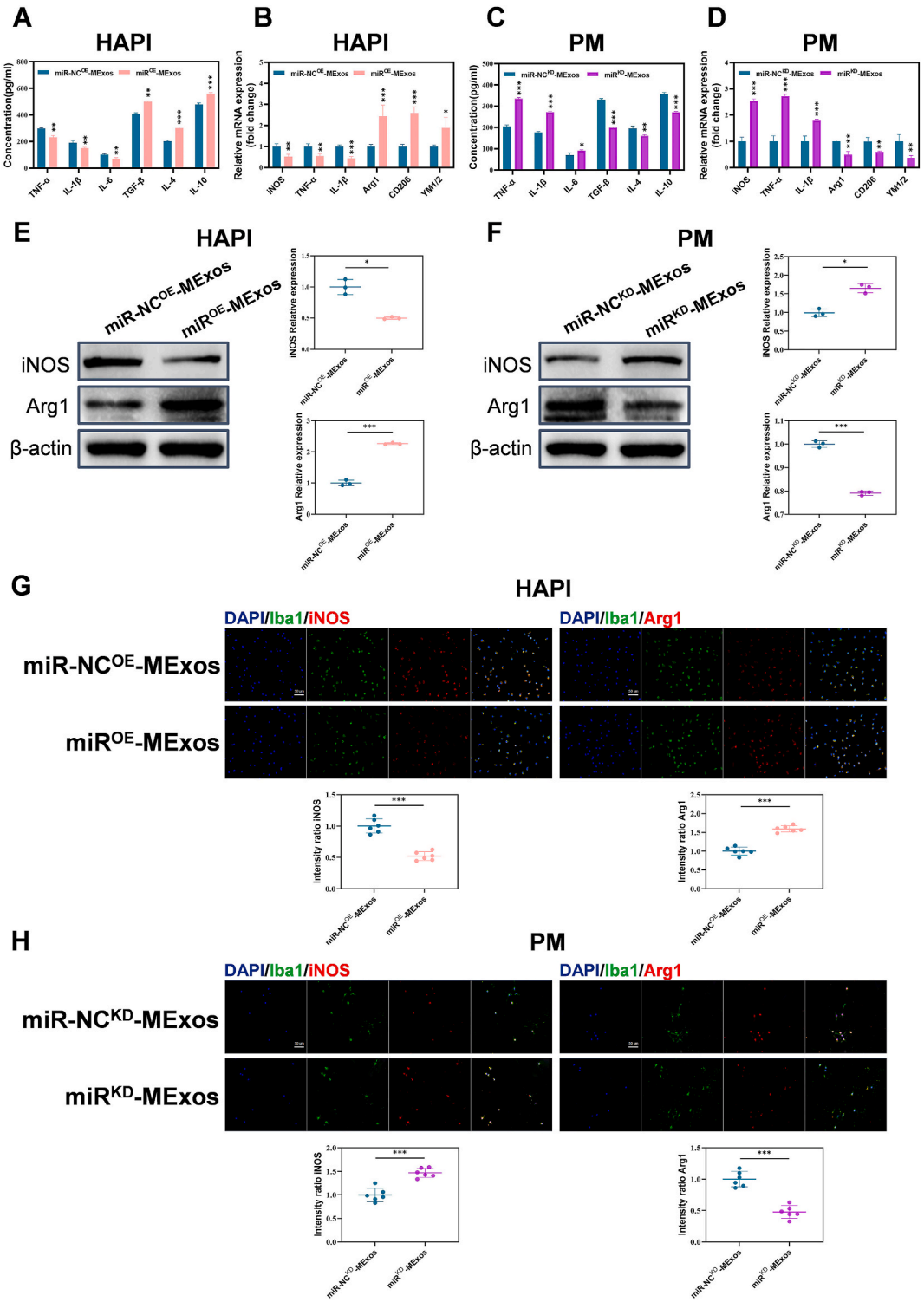

Fig 7. MExos promote microglia polarization from M1 to M2 phenotype via transporting miR-138-5p in vitro. **A** ELISA was utilized to determine cytokine levels in HAPI microglia treated with miR-NC^{OE}-MExos and miR^{OE}-MExos. **B** qRT-PCR was applied to analyze the expression patterns of genes specific to M1/M2 phenotypes in HAPI microglia following treatment with miR-NC^{OE}-MExos and miR^{OE}-MExos. **C** The cytokine concentrations in primary microglia treated with miR-NC^{KD}-MExos and miR^{KD}-MExos were evaluated using ELISA. **D** The gene expression related to M1/M2 phenotypes in primary microglia treated with miR-NC^{KD}-MExos and miR^{KD}-MExos was examined through qRT-PCR. **E** WB analysis was conducted to measure M1/M2 phenotype-specific protein levels in HAPI microglia treated with miR-NC^{OE}-MExos and miR^{OE}-MExos. **F** WB was performed to examine the levels of M1/2 phenotype-specific proteins in primary microglia treated with miR-NC^{KD}-MExos and miR^{KD}-MExos. **G, H** Immunofluorescence imaging and subsequent quantification were carried out to evaluate Arg1 and iNOS in both HAPI and primary microglia treated with miR-NC^{OE}-MExos, miR^{OE}-MExos, miR-NC^{KD}-MExos, and miR^{KD}-MExos. *$p < 0.05$, **$p < 0.01$, ***$p < 0.001$.

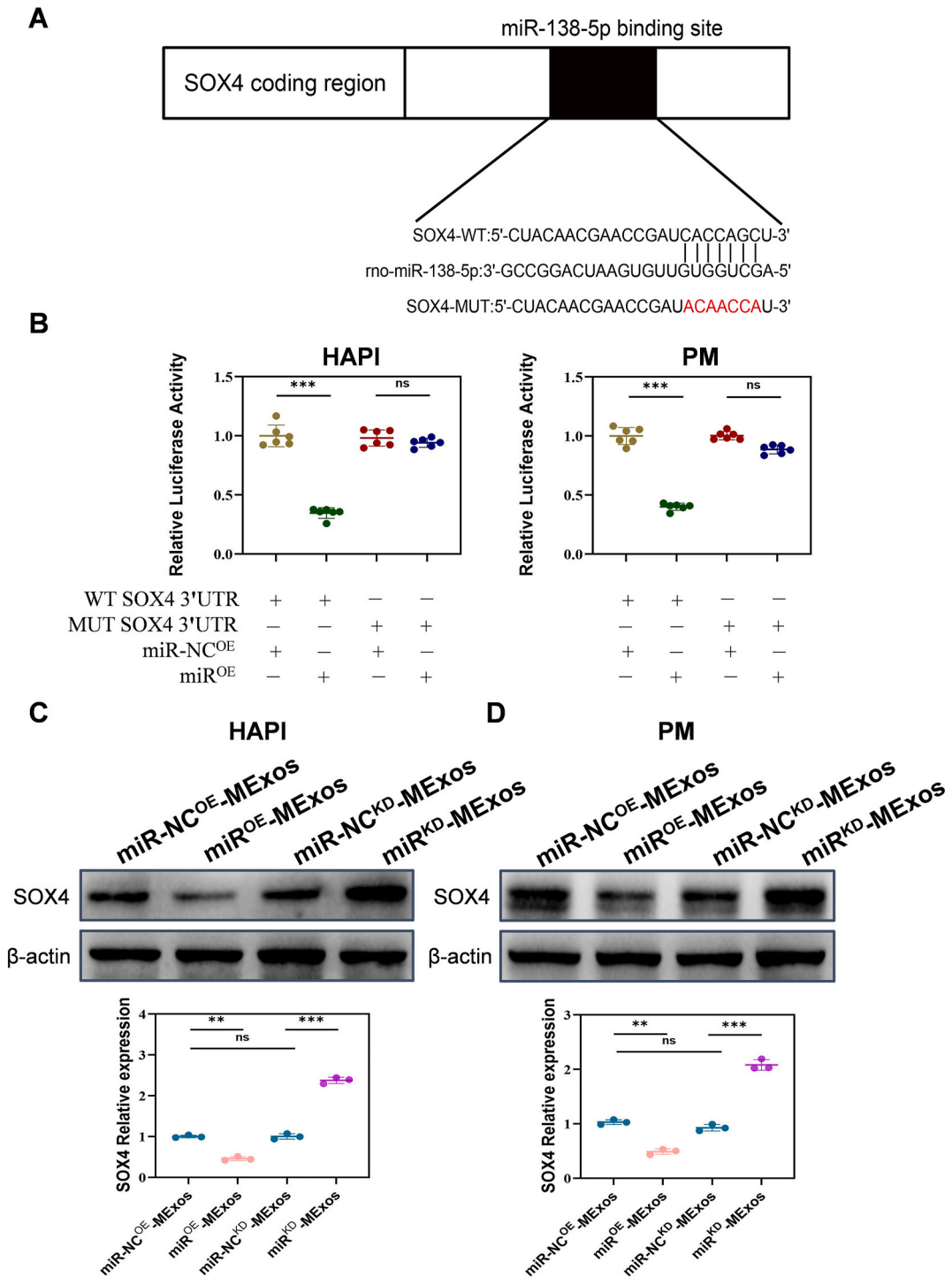

Fig 8. miR-138-5p in MExos directly targets 3′UTR to regulate SOX4. **A, B** Luciferase reporter assay confirmed that SOX4 was the target gene of miR-138-5p. **C** WB analysis showed the inhibition effect of miR-138-5p on SOX4 expression in HAPI microglia. **D** WB analysis demonstrated the inhibition effect of miR-138-5p on SOX4 expression in primary microglia. *p < 0.05, **p < 0.01, ***p < 0.001, ns = no significance.

mediated silencing in HAPI microglia and PM, we assessed the effects of SOX4 on microglia polarization. ELISA results (Fig. 9A) revealed that SOX4 augmentation resulted in an increased release of proinflammatory cytokines, including TNF-α ($p < 0.01$), IL-1β ($p < 0.001$), and IL-6 ($p < 0.001$), and a decrease in anti-inflammatory cytokines like TGF-β ($p < 0.01$), IL-4 ($p < 0.05$), and IL-10 ($p < 0.001$). Conversely, SOX4 knockdown exhibited inverse effects (Fig. 9C, $p < 0.05$). Subsequent analysis using qRT-PCR, WB, and IF confirmed these findings. Specifically, SOX4 overexpression was shown to counteract the microglia phenotype modulation induced by miR^{OE}-MExos, promoting a shift from M2 to M1 polarization in HAPI microglia (Fig. 9B, $p < 0.01$; Fig. 9E, $p < 0.001$; Fig. 9G, $p < 0.001$). In parallel, the adverse effects of miR^{KD}-MExos in PM were mitigated by SOX4 suppression (Fig. 9D, $p < 0.01$; Fig. 9F, $p < 0.001$; Fig. 9H, $p < 0.001$). These results align with our initial hypothesis, affirming the regulatory role of miR-138-5p in microglia polarization via targeting SOX4.

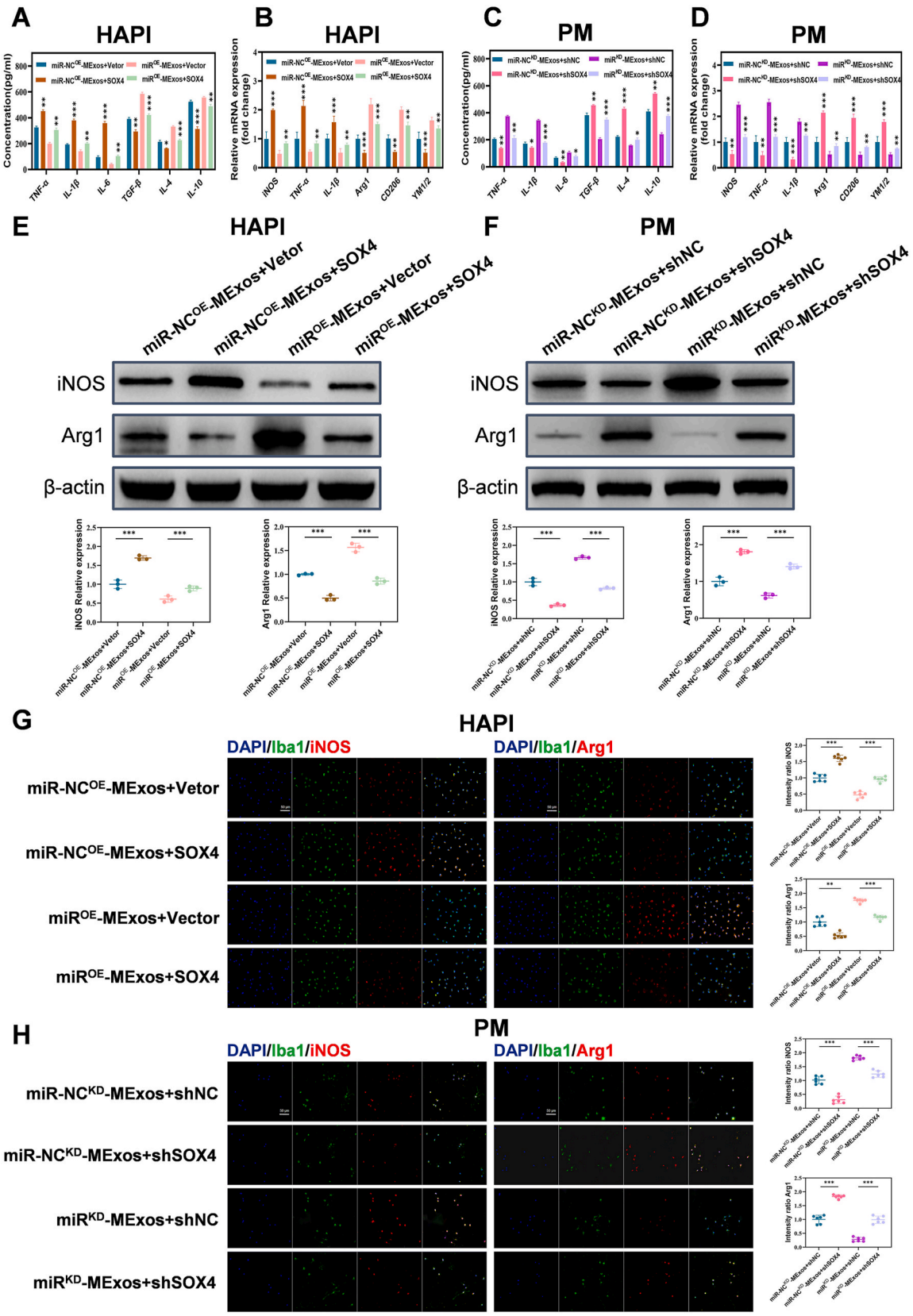

Fig 9. MExos-shuttled miR-138-5p regulates microglia polarization by targeting SOX4. **A, C** ELISA was carried out to substantiate the effects of miR-138-5p inhibition or overexpression, as well as SOX4 knockdown or overexpression, on the levels of inflammatory cytokines in both HAPI microglia and PM cultures. **B, D** The ramifications of miR-138-5p modulation (either inhibition or overexpression) and SOX4 alteration (knockdown or overexpression) on M1/M2-specific gene expression were corroborated via qRT-PCR in both HAPI and PM cells. **E, F** WB was employed to examine the influence of miR-138-5p and SOX4 interventions on the expression levels of M1/M2-specific proteins within HAPI and PM. **G, H** Representative immunofluorescence was utilized to visualize and quantitatively analyze the expression of iNOS and Arg1 in HAPI and PM following the experimental modulation of miR-138-5p and SOX4. *p < 0.05, **p < 0.01, and ***p < 0.001.

4. Discussion

Neuroinflammation is a major pathological process leading to secondary SCI injury [34,35]. Residential microglia, the main inflammatory subpopulations, gear their pathological mechanisms within minutes following the primary injury. Depending on the polarization status of microglia, the post-injury inflammatory response is either neuroprotective or neurotoxic [36,37]. This dual role highlights the need of selectively ablating deleterious M1 microglia and preserving beneficial M2 microglia for treating SCI. Nevertheless, no current anti-inflammatory treatments can reach this goal. In this study, we demonstrated that administration of MExos can shift microglia polarization from M1 to M2 phenotype by targeting miR-138-5p/SOX4 axis and ultimately create a protective microenvironment to counteract the progression of the secondary injury.

Increasing evidences suggest that exosomes serve as carriers for diverse proteins, lipids, nucleic acids, and small regulatory RNAs, playing a pivotal role in cellular communication and physiological processes [38,39]. Moreover, exosomes derived from various cellular sources, notably stem cells, have shown promising outcomes in SCI repair through modulating immune responses, angiogenesis, and axonal regeneration, ultimately contributing to glial scar diminution and functional recovery [40,41]. However, the limited production of exosomes may result in unsatisfactory therapeutic outcomes. Exosomes derived from cell-free sources, such as plasma, present a viable alternative, offering access to potentially larger quantities. Additionally, it has been observed that preconditioned methods can enhance both the yield and functionality of exosomes. In our study, rat models were pretreated with melatonin in order to potentially improve the yield and efficacy of exosomes.

Melatonin is an important neuroendocrine hormone secreted by the pineal gland. It possesses the advantages of low toxicity, high lipid solubility, and crossing cell membranes as well as the blood spinal cord barrier [42]. Besides, melatonin and its metabolites are believed to have significant antioxidant effects, including scavenging oxygen free radicals, activating antioxidant enzymes, reducing oxidative stress, inhibiting inflammation, and preventing cell apoptosis [43]. Previous studies have suggested that melatonin can mitigate liver damage induced by aflatoxin B1 through modulating the TLR4 signaling pathway [44]. Zhang et al. also found that melatonin could alleviate myocardial ischemia-reperfusion injury via improving mitochondrial fusion/mitophagy [45]. However, the application of melatonin in SCI treatment is not widely documented, and its effects on exosomes are to be explored.

This research uncovered a substantial enhancement in both the yield and functionality of Exos following pretreatment with melatonin. Following this discovery, we employed MExos in the treatment of SCI rats, with careful monitoring of their subsequent prognosis. Various behavioral experiments, including BBB score, footprint analysis, and swimming test, confirmed that MExos showed notable improvement in motor function recovery when compared to the Exos group. Similarly, the pathological change of spinal cord on MRI also validated that MExos had a superior capacity in relieving edema of spinal cord tissue. Considering the significant influence of microglia polarization on neuroinflammation and neural restoration in SCI, we proceeded to examine the effect of MExos on the microglia polarization. The anti-inflammatory effects of MExos were confirmed through in vivo experiments, which demonstrated a significant decrease in the expression of proinflammatory cytokines and an increase in the expression of anti-inflammatory factors. Additionally, we examined the effects of MExos on M1/M2 markers. WB and IF staining revealed that MExos were able to suppress the expression of iNOS, a marker for M1 microglia, while enhancing the expression of Arg1, a marker for M2 microglia. We also validated these results through in vitro experiments, and obtained consistent outcomes. These findings underscore the potential of MExos as a significant biological agent for enhancing functional recovery by altering the microglia polarization spectrum from M1 to M2 in rat models of SCI.

MicroRNAs (miRNAs or miRs), which are small non-coding RNAs typically not involved in protein encoding, can regulate an extensive array of target genes [46,47]. These miRNAs are pivotal in various cellular processes such as autophagy, pyroptosis, apoptosis, metabolism, and immune responses, and are increasingly being explored as potential biomarkers for a variety of diseases, including SCI [48,49]. MiRNAs are crucial molecules encapsulated in exosomes and play a significant role in the functional dynamics of these vesicles. After confirming that the functional phenotype of MExos is superior to that of Exos, our research progressed towards unraveling the mechanisms responsible for the observed disparities between these two exosome types. We acquired miRNA profiles from the GEO database (GSE147578) and identified miR-138-5p as one of the miRNAs that was significantly upregulated in MExos.

MiR-138-5p has been extensively studied in various injuries. For instance, researchers have found that MSC-derived exosomes can improve myocardial cell apoptosis and myocardial infarction through the miR-138-5p/SIRT1 axis [50]. Exosome derived from MSC alleviates pathological scars via delivering miR-138-5p to target SIRT1 [51]. However, no research has been reported on the mechanism by which MExos deliver miR-138-5p and regulate microglia polarization after SCI. Through a series of extensive experimental studies, encompassing both in vivo and in vitro methodologies, our research discerned that inhibiting miR-138-5p within MExos effectively negated their therapeutic potential in the management of SCI. Conversely, the upregulation of miR-138-5p in MExos was correlated with an enhancement of their beneficial impact. Consequently, our findings substantiate that engineered MExos enriched with miR-138-5p are instrumental in facilitating the transition of microglia from the M1 to M2 phenotype, thereby contributing to neurological recuperation post-SCI.

MiRNAs typically exert regulatory control over target genes by binding to non-coding regions, leading to translation inhibition and gene expression modulation. In exploring the mechanisms behind exosomal miR-138-5p action, we utilized bioinformatics tools for identifying its potential target gene, pinpointing SOX4 for in-depth analysis. Validation of SOX4 as a target was achieved using a luciferase reporter assay. WB analyses indicated a decrease in SOX4 protein levels following miR-138-5p overexpression, and an increase upon its inhibition in HAPI and PM. Previous studies have indicated that SOX4, under high glucose conditions, exacerbates inflammation and angiogenesis in retinal endothelial cells through NF-κB pathway activation [52]. Additionally, SOX4 suppression has been linked to myocardial ischemia-reperfusion injury mitigation [53]. In our research, we conducted a series of functional assays to corroborate SOX4's role as the target of the identified miRNA. The experiments revealed that SOX4 overexpression microglia negated the beneficial impacts of miR-138-5p overexpression in MExos, while SOX4 knockdown nullified the adverse effects of miR-138-5p inhibition in MExos. Our findings collectively establish that miR-138-5p from MExos attenuates microglia-mediated neuroinflammation by promoting a shift from M1 to M2 microglia polarization, concurrently inhibiting the SOX4 signaling pathway.

Despite the above encouraging findings in this study, some studies have described the miRNA-like off-target effects [54], which might have potential effects on the interpretation of our outcomes. MiRNA-like off-target effects are recognized as siRNA-induced sequence-dependent regulation of unintended transcripts to develop false-positive phenotypes. Such off-target effects follow the same dose response as on-target effects and therefore cannot be selectively eliminated by reducing siRNA concentration, but can be mitigated by siRNA redundancy, siRNA pooling or chemical modification [55–57]. In the present study, siRNA redundancy was used in the relevant experiments with the attempt to overcome such off-target effects.

The clinical translation of exosomes faces many challenges such as massive production, standard isolation, drug loading, stability and quality control. In recent years, artificial exosomes are emerging based

on nanobiotechnology to overcome the limitations of natural exosomes. Major types of artificial exosomes include 'nanovesicles (NVs)', 'exosome-mimetic (EM)' and 'hybrid exosomes (HEs)', which are obtained by top-down, bottom-up and biohybrid strategies, respectively. Artificial exosomes are powerful alternatives to natural exosomes for drug delivery.

5. Conclusion

In a pioneering endeavor, we have procured exosomes from the plasma of rats. Notably, post-administration of melatonin in these rats, we observed that MExos manifested an augmented anti-inflammatory potential along with an enhanced capacity to modulate microglia polarization. A salient elevation in the levels of miR-138-5p within the Exos was discerned subsequent to melatonin treatment, which further attenuated the expression of SOX4 to inhibit its proinflammatory and degeneration processes by regulating microglia polarization. Therefore, our study elucidates the intricate mechanistic pathway by which engineered MExos can modulate microglia polarization, thereby introducing a novel therapeutic avenue for SCI intervention. It is imperative to acknowledge the limitations inherent in our research, given that exosomes are vectors for a multitude of substances, and the current study has delineated only a singular potential pathway of their multifaceted functions. In addition, the clinical translation of exosomes faces many challenges such as massive production, standard isolation, drug loading, stability, quality control and safety [58]. Further studies are required to overcome such obstacles to promote the potential clinical application of exosomes.

Author contributions

BWW, WX, YXW, JY and HC designed and supervised this study. HC, HHS and YQY conducted the majority of the experiments and completed the manuscript. PCW, XZC, LZ, JC and JJH analyzed the data. SFZ, AYL and JXY participated the experiments and the manuscript writing. ZQZ and XMF participated in editing the manuscript. All authors agree and approve the final manuscript.

Ethics approval and consent to participate

All animal procedures were performed under the guidelines of the institutional review board and the ethics committee of Northern Jiangsu People's Hospital.

Consent for publication

Not applicable.

Funding

This work was sponsored by the National Natural Science Foundation of China (82072423, 82272502), the Natural Science Foundation of Jiangsu Province (BK20230294), the Postgraduate Research & Practice Innovation Program of Jiangsu Province (SJCX22-1821) and the Natural Science Foundation of Yangzhou City (SZR2023000040).

Availability of data and materials

The datasets analyzed during the current study are publicly available and can be obtained from the corresponding author upon reasonable request.

Declaration of Competing interest

The authors declare no confict of interest.

Acknowledgements

Thanks to GEO database for their work.

Appendix A. Supplementary data

Supplementary data to this article can be found online at https://doi.org/10.1016/j.jot.2024.09.007.

Abbreviations

SCI	Spinal cord injury
Exos	Plasma-derived exosomes
MExos	Melatonin-pretreated plasma-derived exosomes
CNS	Central nervous system
MSC	Mesenchymal stem cells
ATCC	American type culture collection
DMSO	Dimethyl sulfoxide
TEM	Transmission electron microscopy
NTA	Nanoparticle tracking analysis
WB	Western blot
PBS	Phosphate buffered saline
SD	Sprague–Dawley
BBB	Basso, beattie, and bresnahan
LSS	Louisville swimming scale
EMG	Electromyography
MEP	Motor evoked potential
SD	Standard deviation
MBP	Myelin Basic Protein
NF200	200 kDa subunit of neurofilament
WT	Wild-type
MUT	Mutated
PM	Primary microglia
HAPI	Highly aggressively proliferating immortalize
GEO	Gene expression omnibus

References

[1] Ahuja CS, Wilson JR, Nori S, Kotter MRN, Druschel C, Curt A, et al. Traumatic spinal cord injury. Nat Rev Dis Primers 2017;3:17018.
[2] Anjum A, Yazid MD, Fauzi Daud M, Idris J, Ng AMH, Selvi Naicker A, et al. Spinal cord injury: pathophysiology, multimolecular interactions, and underlying recovery mechanisms. Int J Mol Sci 2020;21:7533.
[3] Karsy M, Hawryluk G. Modern medical management of spinal cord injury. Curr Neurol Neurosci Rep 2019;19:65.
[4] Ahuja CS, Nori S, Tetreault L, Wilson J, Kwon B, Harrop J, et al. Traumatic spinal cord injury-repair and regeneration. Neurosurgery 2017;80:S9–22.
[5] Salter MW, Beggs S. Sublime microglia: expanding roles for the guardians of the CNS. Cell 2014;158:15–24.
[6] Paolicelli RC, Bolasco G, Pagani F, Maggi L, Scianni M, Panzanelli P, et al. Synaptic pruning by microglia is necessary for normal brain development. Science. 2011;333:1456–8.
[7] Wake H, Moorhouse AJ, Jinno S, Kohsaka S, Nabekura J. Resting microglia directly monitor the functional state of synapses in vivo and determine the fate of ischemic terminals. J Neurosci 2009;29:3974–80.
[8] Fang Y-P, Qin Z-H, Zhang Y, Ning B. Implications of microglial heterogeneity in spinal cord injury progression and therapy. Exp Neurol 2023;359:114239.
[9] Tu H, Chu H, Guan S, Hao F, Xu N, Zhao Z, et al. The role of the M1/M2 microglia in the process from cancer pain to morphine tolerance. Tissue Cell 2021;68:101438.
[10] Colonna M, Butovsky O. Microglia function in the central nervous system during Health and neurodegeneration. Annu Rev Immunol 2017;35:441–68.
[11] Hanisch U-K, Kettenmann H. Microglia: active sensor and versatile effector cells in the normal and pathologic brain. Nat Neurosci 2007;10:1387–94.
[12] Shen K, Sun G, Chan L, He L, Li X, Yang S, et al. Anti-inflammatory nanotherapeutics by targeting matrix metalloproteinases for immunotherapy of spinal cord injury. Small 2021;17:e2102102.
[13] Saijo K, Crotti A, Glass CK. Regulation of microglia activation and deactivation by nuclear receptors. Glia 2013;61:104–11.
[14] Pegtel DM, Gould SJ. Exosomes. Annu Rev Biochem. 2019;88:487–514.
[15] Kalluri R, LeBleu VS. The biology, function, and biomedical applications of exosomes. Science 2020;367:eaau6977.

[16] Kimiz-Gebologlu I, Oncel SS. Exosomes: large-scale production, isolation, drug loading efficiency, and biodistribution and uptake. J Control Release 2022;347:533–43.
[17] Tenchov R, Sasso JM, Wang X, Liaw W-S, Chen C-A, Zhou QA. Exosomes—Nature's lipid nanoparticles, a rising star in drug delivery and diagnostics. ACS Nano 2022;16:17802–46.
[18] Fan L, Liu C, Chen X, Zheng L, Zou Y, Wen H, et al. Exosomes-Loaded electroconductive hydrogel synergistically promotes tissue repair after spinal cord injury via immunoregulation and enhancement of myelinated axon growth. Adv Sci 2022;9:e2105586.
[19] Liu W-Z, Ma Z-J, Li J-R, Kang X-W. Mesenchymal stem cell-derived exosomes: therapeutic opportunities and challenges for spinal cord injury. Stem Cell Res Ther 2021;12:102.
[20] Liu W, Wang Y, Gong F, Rong Y, Luo Y, Tang P, et al. Exosomes derived from bone mesenchymal stem cells repair traumatic spinal cord injury by suppressing the activation of A1 neurotoxic reactive astrocytes. J Neurotrauma 2019;36:469–84.
[21] Hwang J, Jang S, Kim C, Lee S, Jeong H-S. Role of stem cell-derived exosomes and microRNAs in spinal cord injury. Int J Mol Sci 2023;24:13849.
[22] Vicencio JM, Yellon DM, Sivaraman V, Das D, Boi-Doku C, Arjun S, et al. Plasma exosomes protect the myocardium from ischemia-reperfusion injury. J Am Coll Cardiol 2015;65:1525–36.
[23] Zhou Z, Wang R, Wang J, Hao Y, Xie Q, Wang L, et al. Melatonin pretreatment on exosomes: heterogeneity, therapeutic effects, and usage. Front Immunol 2022;13:933736.
[24] Liang G, Zhu Y, Ali DJ, Tian T, Xu H, Si K, et al. Engineered exosomes for targeted co-delivery of miR-21 inhibitor and chemotherapeutics to reverse drug resistance in colon cancer. J Nanobiotechnology 2020;18:10.
[25] Yu M, Liu W, Li J, Lu J, Lu H, Jia W, et al. Exosomes derived from atorvastatin-pretreated MSC accelerate diabetic wound repair by enhancing angiogenesis via AKT/eNOS pathway. Stem Cell Res Ther 2020;11:350.
[26] Liu W, Rong Y, Wang J, Zhou Z, Ge X, Ji C, et al. Exosome-shuttled miR-216a-5p from hypoxic preconditioned mesenchymal stem cells repair traumatic spinal cord injury by shifting microglial M1/M2 polarization. J Neuroinflammation 2020;17:47.
[27] Liu W, Yu M, Xie D, Wang L, Ye C, Zhu Q, et al. Melatonin-stimulated MSC-derived exosomes improve diabetic wound healing through regulating macrophage M1 and M2 polarization by targeting the PTEN/AKT pathway. Stem Cell Res Ther 2020;11:259.
[28] Wang J, Chen D, Ho EA. Challenges in the development and establishment of exosome-based drug delivery systems. J Control Release 2021;329:894–906.
[29] Novais AA, Chuffa LG de A, Zuccari DAP de C, Reiter RJ. Exosomes and melatonin: where their destinies intersect. Front Immunol 2021;12:692022.
[30] Yin N, Zhao Y, Liu C, Yang Y, Wang Z-H, Yu W, et al. Engineered nanoerythrocytes alleviate central nervous system inflammation by regulating the polarization of inflammatory microglia. Adv Mater 2022;34:e2201322.
[31] Lu W, Yan J, Wang C, Qin W, Han X, Qin Z, et al. Interorgan communication in neurogenic heterotopic ossification: the role of brain-derived extracellular vesicles. Bone Res. 2024;12:11.
[32] Yan J, Gao B, Wang C, Lu W, Qin W, Han X, et al. Calcified apoptotic vesicles from PROCR+ fibroblasts initiate heterotopic ossification. J Extracell Vesicles 2024;13:e12425.
[33] Li W, Chen J, Zhao S, Huang T, Ying H, Trujillo C, et al. High drug-loaded microspheres enabled by controlled in-droplet precipitation promote functional recovery after spinal cord injury. Nat Commun [Internet] 2022;13:1262 [cited 2024 Jan 3], https://www.ncbi.nlm.nih.gov/pmc/articles/PMC8913677/.
[34] Hellenbrand DJ, Quinn CM, Piper ZJ, Morehouse CN, Fixel JA, Hanna AS. Inflammation after spinal cord injury: a review of the critical timeline of signaling cues and cellular infiltration. J Neuroinflammation 2021;18:284.
[35] Shao A, Tu S, Lu J, Zhang J. Crosstalk between stem cell and spinal cord injury: pathophysiology and treatment strategies. Stem Cell Res Ther 2019;10:238.
[36] Guo S, Wang H, Yin Y. Microglia polarization from M1 to M2 in neurodegenerative diseases. Front Aging Neurosci 2022;14:815347.
[37] Shao F, Wang X, Wu H, Wu Q, Zhang J. Microglia and neuroinflammation: crucial pathological mechanisms in traumatic brain injury-induced neurodegeneration. Front Aging Neurosci 2022;14:825086.
[38] Chen X, Wan Z, Yang L, Song S, Fu Z, Tang K, et al. Exosomes derived from reparative M2-like macrophages prevent bone loss in murine periodontitis models via IL-10 mRNA. J Nanobiotechnology 2022;20:110.
[39] Zhang H, Jin K. Peripheral circulating exosomal miRNAs potentially contribute to the regulation of molecular signaling networks in aging. Int J Mol Sci [Internet] 2020;21:1908 [cited 2024 Jan 3], https://www.ncbi.nlm.nih.gov/pmc/articles/PMC7139634/.
[40] Xiong W, Li C, Kong G, Zeng Q, Wang S, Yin G, et al. Treg cell-derived exosomes miR-709 attenuates microglia pyroptosis and promotes motor function recovery after spinal cord injury. J Nanobiotechnology 2022;20:529.
[41] Ren Z, Qi Y, Sun S, Tao Y, Shi R. Mesenchymal stem cell-derived exosomes: hope for spinal cord injury repair. Stem Cells Dev. 2020;29:1467–78.
[42] Gorman MR. Temporal organization of pineal melatonin signaling in mammals. Mol Cell Endocrinol 2020;503:110687.
[43] Manchester LC, Coto-Montes A, Boga JA, Andersen LPH, Zhou Z, Galano A, et al. Melatonin: an ancient molecule that makes oxygen metabolically tolerable. J Pineal Res 2015;59:403–19.
[44] Liu S, Kang W, Mao X, Ge L, Du H, Li J, et al. Melatonin mitigates aflatoxin B1-induced liver injury via modulation of gut microbiota/intestinal FXR/liver TLR4 signaling axis in mice. J Pineal Res 2022;73:e12812.
[45] Zhang Y, Wang Y, Xu J, Tian F, Hu S, Chen Y, et al. Melatonin attenuates myocardial ischemia-reperfusion injury via improving mitochondrial fusion/mitophagy and activating the AMPK-OPA1 signaling pathways. J Pineal Res 2019;66:e12542.
[46] Guarnieri DJ, DiLeone RJ. MicroRNAs: a new class of gene regulators. Ann Med 2008;40:197–208.
[47] Esquela-Kerscher A, Slack FJ. Oncomirs - microRNAs with a role in cancer. Nat Rev Cancer 2006;6:259–69.
[48] Hatfield S, Ruohola-Baker H. microRNA and stem cell function. Cell Tissue Res 2008;331:57–66.
[49] Bi Y, Liu G, Yang R. MicroRNAs: novel regulators during the immune response. J Cell Physiol 2009;218:467–72.
[50] Mao Q, Liang X-L, Zhang C-L, Pang Y-H, Lu Y-X. LncRNA KLF3-AS1 in human mesenchymal stem cell-derived exosomes ameliorates pyroptosis of cardiomyocytes and myocardial infarction through miR-138-5p/Sirt1 axis. Stem Cell Res Ther 2019;10:393.
[51] Zhao W, Zhang R, Zang C, Zhang L, Zhao R, Li Q, et al. Exosome derived from mesenchymal stem cells alleviates pathological scars by inhibiting the proliferation, migration and protein expression of fibroblasts via delivering miR-138-5p to target SIRT1. Int J Nanomedicine 2022;17:4023–38.
[52] Wei H, Gu Q. SOX4 promotes high-glucose-induced inflammation and angiogenesis of retinal endothelial cells by activating NF-κB signaling pathway. Open Life Sci 2022;17:393–400.
[53] Zhang L, Lv L, Zheng N, Li R, Yang R, Li T, et al. Suppression of Sox4 protects against myocardial ischemic injury by reduction of cardiac apoptosis in mice. J Cell Physiol 2021;236:1094–104.
[54] Seok H, Lee H, Jang E-S, Chi SW. Evaluation and control of miRNA-like off-target repression for RNA interference. Cell Mol Life Sci 2018;75:797–814.
[55] Jackson AL, Linsley PS. Recognizing and avoiding siRNA off-target effects for target identification and therapeutic application. Nat Rev Drug Discov 2010;9:57–67.
[56] Singh S, Narang AS, Mahato RI. Subcellular fate and off-target effects of siRNA, shRNA, and miRNA. Pharm Res (N Y) 2011;28:2996–3015.
[57] Kobayashi Y, Tian S, Ui-Tei K. The siRNA off-target effect is determined by base-pairing stabilities of two different regions with opposite effects. Genes 2022;13:319.
[58] Li Y-J, Wu J-Y, Liu J, Xu W, Qiu X, Huang S, et al. Artificial exosomes for translational nanomedicine. J Nanobiotechnology 2021;19:242.